A PWM Method of H-Bridge Converter With Temperature Rise Balancing and Minimization Based on Periodically Alternating Employment of Power Devices

Cong Wang, Changgeng Tian, Hong Cheng, and Jiaqing Deng

***Abstract*—Aiming at the temperature rise and thermal control issues of power devices in H-bridge converters under conventional pulsewidth modulation (PWM) methods, a novel PWM method of H-bridge converter with temperature rise balancing and minimization based on periodically alternating employment of power devices is proposed. In the proposed method, two novel operation mechanisms of power devices are alternately applied into the eight regions with the identical and opposite polarities of reference voltage and input current, which are composed of two fundamental frequency periods. All active switches and antiparallel diodes in H-bridge converters are made to work alternately in these eight regions, each of them is designed to keep in ON-state in one region, operate in switching state in another two regions, and inactive in the left other five regions. This way, the power dissipation and temperature rise of all the devices are balanced and minimized, and H-bridge converters no longer suffer from the dead-time effect on current quality and dc-bus voltage utilization. The implementation strategy of the proposed modulation method is discussed in detail. Simulation and experimental results are presented that verify the effectiveness of the proposed method and the corresponding implementation strategy at different operating points.**

***Index Terms*—H-bridge converter, junction temperature reduction, operation mechanisms of power devices, power dissipation mitigation, pulse width modulation, temperature rise.**

I. Introduction

With the rapid development of power electronics and the continuous progress of industrial modernization, multilevel power converters have been increasingly applied in the fields of high-voltage direct current transmission system (HVDC) [1], active power filter system [2], reactive power compensation system [3], [4], and high-voltage and high-power frequency conversion speed regulation system [5]. Among the various circuit topologies of multilevel converters, the cascaded topology represented by the cascaded H-bridge multilevel converters has gradually become the mainstream of the market because of its significant advantages, such as modular design, low harmonic pollution, wide input and output power range, easy system expansion, and redundant control. It is widely applied in medium- and high-voltage power electronic transformers [6], novel transformerless cascaded medium- and high-voltage converters [7], static var generators [8]–[10], and modular multilevel converters [11], [12]. However, the main problem of these power electronic systems composed of cascaded H-bridge converters in practical applications is the high failure rate and low reliability of their cascaded cells. In recent years, as the power level and the number of cascaded cells of such systems in high-voltage and high-power applications continue to increase, the reliability of fully controlled H-bridge converters has become one of the critical issues affecting their operation performance, which has been extensively studied and discussed [13]–[15].

The investigation shows that the failure of power semiconductor devices is the main factor leading to the reliability issue of H-bridge converters, especially the active power switching devices are not only the most fragile components within H-bridge converters, but also the biggest heat source, and their service lifetime is closely related to the temperature rise of the chips [16], [17]. The temperature rise of the chip in the power switching device is mainly caused by the power losses of the chip itself, and the greater the losses, the higher the temperature rise. Excessive junction temperature and junction temperature fluctuations (especially fundamental frequency and low-frequency junction temperature fluctuations) can cause damage to the silicon chip on one hand, and on the other hand, it will aggravate the thermal–mechanical stress among the layers of materials with mismatched thermal expansion coefficients inside the device, thus accelerating the failure of the device [17]. The relationship among the means junction temperature, junction temperature fluctuations, and the number of insulated gate bipolar transistor (IGBT) thermal cycles based on the Coffin–Manson model is presented in [18], which showed that the lifetime of IGBT decreases significantly with the increase of the means junction temperature and junction temperature fluctuations. Hence, reducing

Manuscript received September 30, 2021; revised November 29, 2021 and February 4, 2022; accepted March 12, 2022. Date of publication March 23, 2022; date of current version May 23, 2022. This work was supported by the National Natural Science Foundation of China under Grant 51577187. Recommended for publication by Associate Editor M. Liserre. *(Corresponding author: Changgeng Tian.)*

The authors are with the School of Mechanical Electronic and Information Engineering, China University of Mining and Technology, Beijing 100083, China (e-mail: wangc@cumtb.edu.cn; 983767044@qq.com; chengh@cumtb.edu.cn; dengjiaqingrae@163.com).

Color versions of one or more figures in this article are available at https://doi.org/10.1109/TPEL.2022.3161665.

Digital Object Identifier 10.1109/TPEL.2022.3161665

the means junction temperature and junction temperature fluctuations will effectively prolong the lifetime of power switching devices and improve the reliability of H-bridge converters.

Currently, a large number of research works have explored junction temperature control methods for power switching devices, mainly including losses compensation methods [19]–[23] and losses reduction methods [24]–[32], known as active thermal control. The basic idea of losses compensation methods is to smooth junction temperature fluctuations by increasing the devices losses when junction temperature is in a downward trend. The corresponding implementation strategies include increasing the switching frequency [19], [20], reducing the driving voltage [21], [22], and introducing the reactive current cycling in the parallel converter system [23]. However, these methods inevitably increased the overall losses and means junction temperature of power devices. The basic idea of losses reduction methods is to reduce the switching losses or evenly distribute the conduction losses to achieve junction temperature management. The corresponding implementation strategies include reducing the switching frequency [24]–[26], dynamically adjusting the dc-bus voltage in the traction drives with permanent magnet synchronous motor (PMSM) [27] and adopting the improved modulation schemes, such as the discontinuous pulsewidth modulation (DPWM) strategy [28]–[30]. However, those methods will significantly increase the current harmonics and reduce the output quality of the H-bridge converter, which is unacceptable in some applications. Ko *et al.* [31] and [32] studied an improved DPWM strategy for a cascaded H-bridge converter system, which reduced the switching losses of the devices in higher aged cell and obtained a comparable THD performance to the common phase-shifted PWM (PS-PWM) strategy. However, the clamping region present in the modulation signal also affected the conduction time, which resulted in an unbalanced conduction losses distribution and junction temperatures distribution among the power devices of higher aged cell. In particular, this imbalance aggravates as the input current and dc-bus voltage increase. Obviously, the previous studies on thermal control have more or less limitations, and there has not been a satisfactory solution that can effectively reduce and uniformly distribute the junction temperature of all power devices in H-bridge converters without affecting the operation performance and output quality. In addition, for conventional bipolar and unipolar pulsewidth modulation (PWM) methods applied to H-bridge converters, the excessive and unbalanced use of power devices and the forced turn-ON of unnecessary switching devices have been two neglected reliability issues that also greatly affect the junction temperature distribution of power switching devices and the output quality of H-bridge converters.

To address the temperature rise and thermal control issues of power devices under conventional PWM methods, this article proposes a novel PWM method with temperature rise balancing and minimization for fully controlled H-bridge converter based on periodically alternating employment of power devices. The proposed method is applicable to all operating points of H-bridge converters, including different current magnitudes, power factors, and fundamental frequencies. By employing each power device evenly and alternately in two fundamental frequency periods, the proposed method not only achieves the effective reduction and uniform distribution of the junction temperature for all power switching devices without altering the switching frequency, but also makes the H-bridge converter no longer suffer from the dead-time effect on the current quality and dc-bus voltage utilization. This article is organized as follows. In Section II, the proposed PWM method based on power devices alternating operation mechanisms is presented. The theoretical losses analysis is investigated in Section III. Simulation and experiment results are presented and discussed in Section IV. Finally, Section V concludes the article.

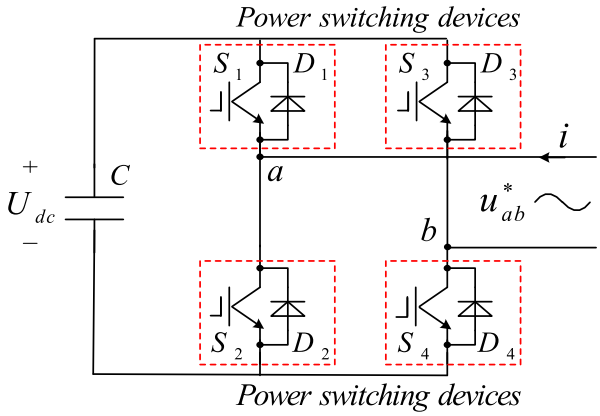

Fig. 1 Circuit configuration of H-bridge converter.

II. Principle of the Proposed PWM Method Based on Power Devices Alternately Employed

The H-bridge converter analyzed in this article, as shown in Fig. 1, contains a dc-side capacitor C, four active power switches $S_1, S_2, S_3, \text{and } S_4$, and four freewheeling diodes $D_1, D_2, D_3, \text{ and } D_4$. Based on the bidirectional power transmission characteristics, the H-bridge converter can operate not only in rectifier mode or inverter mode under programmable leading or lagging power factors, but also in capacitive reactive power compensator (CRPC) mode or inductive reactive power compensator (IRPC) mode. The waveforms of ac-side reference voltage u_{ab}^* and input current i in the four operation modes are shown in Fig. 2, respectively, and the expressions of u_{ab}^* and i are given by (1), where m is the modulation ratio and θ is the phase difference between u_{ab}^* and i

$$\begin{cases} u_{ab}^* = U_{\text{dc}} m \sin(\omega t) \\ i = I_m \sin(\omega t + \theta). \end{cases} \tag{1}$$

It can be observed that the fundamental frequency period T_f of u_{ab}^* can be divided into four regions according to the different polarity characteristics of u_{ab}^* and i regardless of the operation mode, where different modulation modes will generate a variety of operation mechanisms for power devices and determine their usage state.

Bipolar and unipolar modulation are two basic modulation modes adopted in PWM methods for H-bridge converters, which are also the basis for carrier phase-shifted PWM and carrier level-shifted PWM for cascaded H-bridge converters.

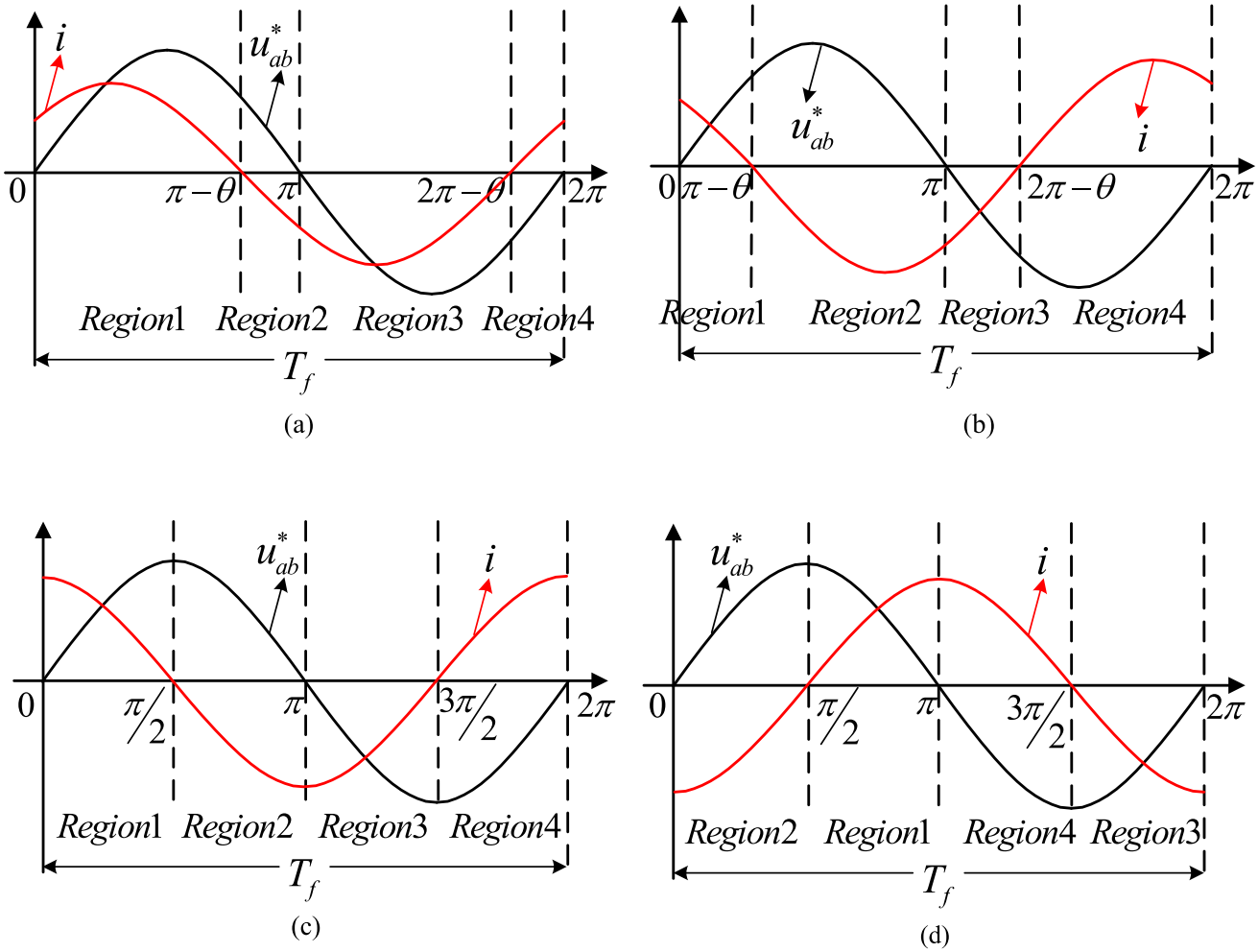

Fig. 2 Waveforms of ac-side reference voltage and input current in four operation modes. (a) Rectifier mode. (b) Inverter mode. (c) CRPC mode. (d) IRPC mode.

However, these two basic modulation modes have the inherent drawbacks in the operation mechanisms generated for power devices, such as unnecessary excessive or unbalanced use of power devices, and the forced turn-ON of unnecessary switching devices. In order to better explain the advantage of the proposed PWM method by this article and for the sake of completeness, the conventional bipolar and unipolar PWM methods are reviewed at first briefly before introducing the proposed PWM method.

A. Brief Review of Conventional PWM Methods

For conventional bipolar PWM method, as shown in Fig. 3(a), a pair of complementary drive signals are generated to control the two pairs of diagonally opposite switches from the two legs, which makes these two pairs of switches switch ON and OFF alternately in one switching cycle $T_{\rm sw}$, and the input voltage fluctuate between two values. The corresponding operation mechanisms of the devices in each region are depicted in Fig. 4, where S_2, S_3 and D_1, D_4 are alternately switched in regions 1 and 4, while S_1, S_4, and D_2, D_3 are alternately switched in regions 2 and 3. The mean conduction time $T_{\rm con}$ of them within T_f are given by the following equation:

$$\begin{cases} T_{\rm con\_}S_2,S_3 = \frac{1}{2\pi}\int_{-\theta}^{\pi-\theta}\left(\frac{1-m\sin\omega t}{2}T_f\right)\cdot d\tau \\ \qquad\qquad = \frac{(\pi-2m\cos\theta)}{4\pi}T_f \\ T_{\rm con\_}D_1,D_4 = \frac{1}{2\pi}\int_{-\theta}^{\pi-\theta}\left(\frac{1+m\sin\omega t}{2}T_f\right)\cdot d\tau \\ \qquad\qquad = \frac{(\pi+2m\cos\theta)}{4\pi}T_f \\ T_{\rm con\_}S_1,S_4 = \frac{1}{2\pi}\int_{\pi-\theta}^{2\pi-\theta}\left(\frac{1+m\sin\omega t}{2}T_f\right)\cdot d\tau \\ \qquad\qquad = \frac{(\pi-2m\cos\theta)}{4\pi}T_f. \\ T_{con\_}D_2,D_3 = \frac{1}{2\pi}\int_{\pi-\theta}^{2\pi-\theta}\left(\frac{1-m\sin\omega t}{2}T_f\right)\cdot d\tau \\ \qquad\qquad = \frac{(\pi+2m\cos\theta)}{4\pi}T_f. \end{cases} \tag{2}$$

Since the sum of the time duration of regions 1 and 4 and that of regions 2 and 3 are both equal to $T_f/2$, the switching times $N_{\rm sw}$ of them within T_f are given by the following equation:

$$N_{\rm sw\_}S_1,S_2,S_3,S_4 = N_{\rm sw\_}D_1,D_2,D_3,D_4 = \frac{T_f}{2T_{\rm sw}}. \tag{3}$$

Obviously, this method makes all switches operate in switching state without a break, which not only increases their

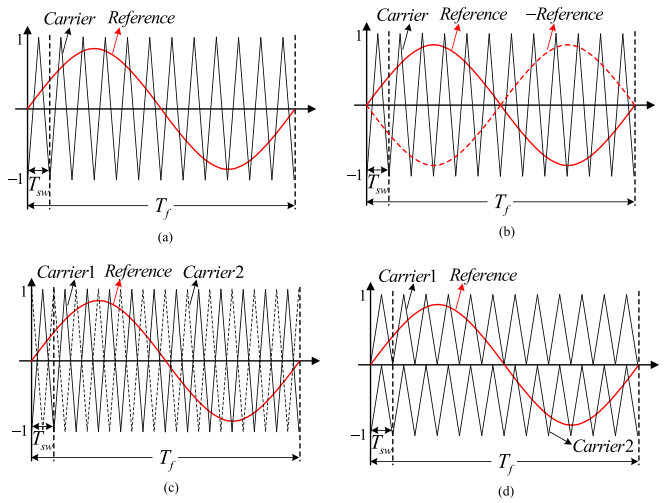

Fig. 3 Conventional PWM modes for H-bridge converter. (a) Bipolar modulation mode. (b) Unipolar-I modulation mode. (c) Unipolar-II modulation mode. (d) Unipolar-III modulation mode.

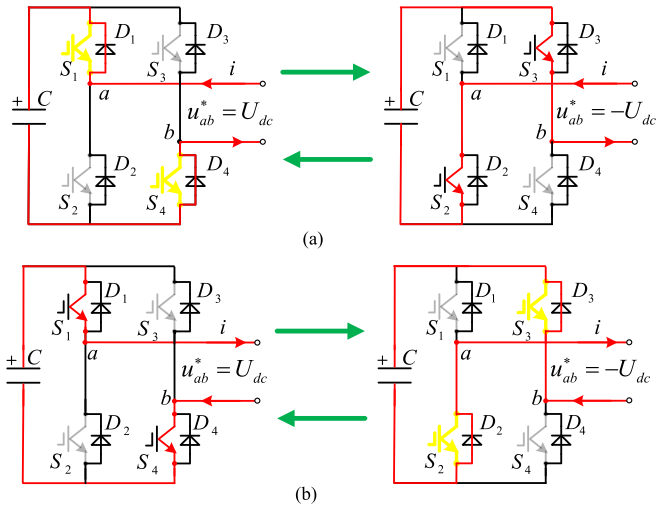

Fig. 4 Operation mechanisms of power devices in each region under bipolar PWM method. (a) In regions 1 and 4. (b) In regions 2 and 3. (a) S_1, S_4, D_1, D_4 and S_2, S_3 operate in switching state. (b) S_1, S_4 and S_2, S_3, D_2, D_3 operate in switching state.

switching losses, but also forces those switches, such as S_1 and S_4 in regions 1 and 4, S_2 and S_3 in regions 2 and 3, to be in unnecessary ON-state.

For conventional unipolar PWM methods, Fig. 3(b)–(d) shows three types of modulation strategies, labeled as I, II, and III, which are characterized by the generation of two pairs of complementary drive signals for left and right legs, respectively, and the input voltage containing three voltage levels. For unipolar-I and II modulation strategies, the operation mechanisms of the devices under them are equivalent to that under bipolar modulation strategy due to the identical switching times and conduction time of each device in each region. For unipolar-III modulation strategy, the devices will possess two operation mechanisms depending on the different distribution of drive signals for the switches, one of which is illustrated in Fig. 5. The switching times $N_{\rm sw}$ and mean conduction time $T_{\rm con}$ of the devices within T_f based on the operation mechanism in Fig. 5 are given by the following equations:

$$\begin{cases} N_{\rm sw\_}S_1,S_3 = N_{\rm sw\_}D_2,D_4 = \frac{(\pi-\theta)T_f}{2\pi T_{\rm sw}} \\ N_{\rm sw\_}S_2,S_4 = N_{\rm sw\_}D_1,D_3 = \frac{(\theta)T_f}{2\pi T_{\rm sw}} \end{cases} \tag{4}$$

$$\begin{cases} T_{\rm con\_}S_1,S_3 = \frac{(\pi-m-m\cos\theta)}{2\pi}T_f \\ T_{\rm con\_}S_2,S_4 = \frac{(m-m\cos\theta)}{2\pi}T_f \\ T_{\rm con\_}D_1,D_3 = \frac{(\pi-m+m\cos\theta)}{2\pi}T_f \\ T_{\rm con\_}D_2,D_4 = \frac{(m+m\cos\theta)}{2\pi}T_f. \end{cases} \tag{5}$$

Obviously, this method makes all the devices have nonuniform switching times and conduction time, it also forces the unnecessary switches to keep working.

The operation mechanisms of all the power devices in each region under conventional bipolar and unipolar PWM methods are summarized in Table I, where it can be seen that these operation mechanisms inevitably bring about an unnecessary growth in power device losses caused by either excessive use or unbalanced use of the devices, and make the converter suffer from the dead-time effect due to those switches kept in unnecessary ON-state, which worsens the reliability and output quality of the H-bridge converter.

B. Novel Mechanisms of the Proposed PWM Method

In response to this issue, this article proposes a novel PWM method for the H-bridge converter with temperature rise balancing and minimization based on periodically alternating employment of power devices, in which two novel mechanisms (type-A and type-B) are proposed and alternated in an alternating cycle composed of two fundamental frequency periods. The proposed PWM method is applicable to all operation modes of H-bridge converters. Taking the CRPC mode illustrated in Fig. 6 as an example, mechanism type-A is applied to four of the eight regions, where reference voltage u_{ab}^* and input current i have identical polarities, while mechanism type-B will be applied to the other four regions, where u_{ab}^* and i have the opposite polarities. The principles of mechanism type-A and type-B will be explained in detail as follows.

As shown in Fig. 7, mechanism type-A is designed for regions 1, 3, 5, and 7, which is characterized by keeping one diode in ON-state, and operating its diagonally opposite diode and a switch (from the other power module in the same leg as the diagonal diode) in the switching state. It can be seen from Fig. 7(a) that the normal PWM operation of the H-bridge converter in region 1 can be achieved only by keeping diode D_1 in the ON-state, and making switch S_3 and diode D_4 operate in switching state, instead of requiring all devices (including necessary and unnecessary devices) to operate in ON-state or switching state as what under traditional PWM methods. In order to evenly use each power device, the proposed method takes two fundamental frequency periods $2T_f$ to constitute the alternating cycle. It can be seen in Fig. 7(c) that the PWM operation in region 5 (first region in second fundamental frequency cycle) is different from

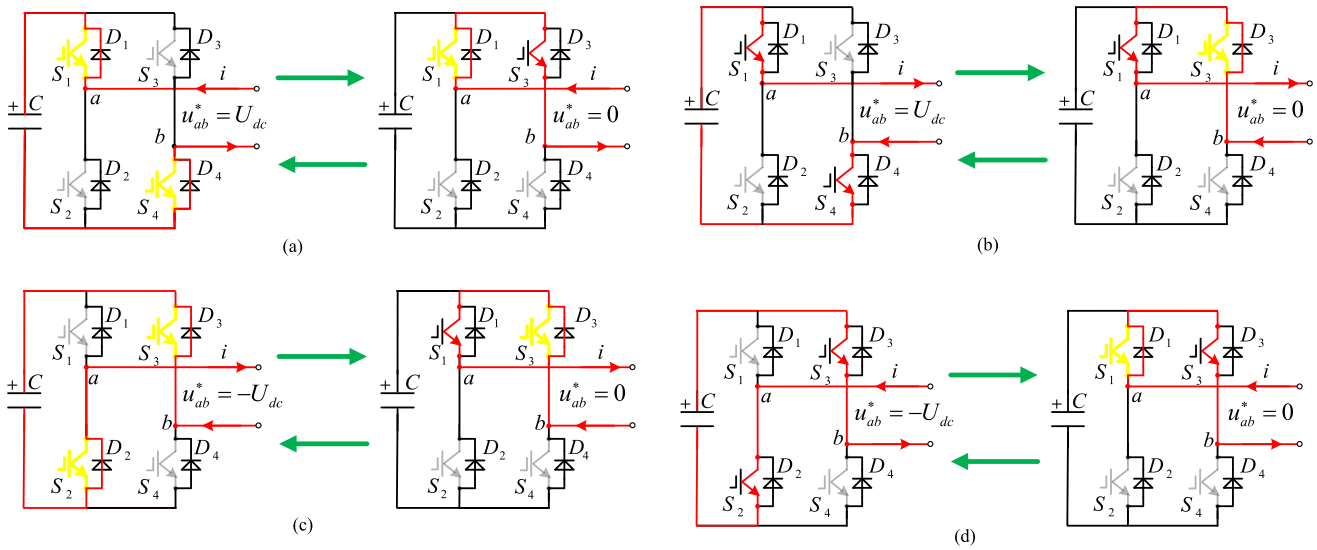

Fig. 5 Operation mechanisms of power devices in each region under unipolar-III PWM method. (a) In region 1. (b) In region 2. (c) In region 3. (d) In region 4. (a) S_1, D_1 keep in on-state, S_4, D_4 and S_3 operate in switching state. (b) S_1 keeps in on-state, S_3, D_3 and S_4 operate in switching state. (c) S_3, D_3 keep in on-state, S_2, D_2 and S_1 operate in switching state. (d) S_3 keeps in on-state, S_1, D_1 and S_2 operate in switching state.

TABLE I
OPERATION MECHANISMS OF POWER DEVICES UNDER CONVENTIONAL PWM METHODS

Regions	Operation mechanisms under bipolar, unipolar-I and II PWM methods	Operation mechanisms under unipolar-III PWM method	
Region 1	S_1, S_4, D_1, D_4 and S_2, S_3 operate in switching state	S_1, D_1 keep in on-state, S_4, D_4 and S_3 operate in switching state	S_4, D_4 keep in on-state, S_1, D_1 and S_2 operate in switching state
Region 2	S_2, S_3, D_2, D_3 and S_1, S_4 operate in switching state	S_1 keeps in on-state, S_3, D_3 and S_4 operate in switching state	S_4 keeps in on-state, S_2, D_2 and S_1 operate in switching state
Region 3	S_2, S_3, D_2, D_3 and S_1, S_4 operate in switching state	S_3, D_3 keep in on-state, S_2, D_2 and S_1 operate in switching state	S_2, D_2 keep in on-state, S_3, D_3 and S_4 operate in switching state
Region 4	S_1, S_4, D_1, D_4 and S_2, S_3 operate in switching state	S_3 keeps in on-state, S_1, D_1 and S_2 operate in switching state	S_2 keeps in on-state, S_4, D_4 and S_3 operate in switching state

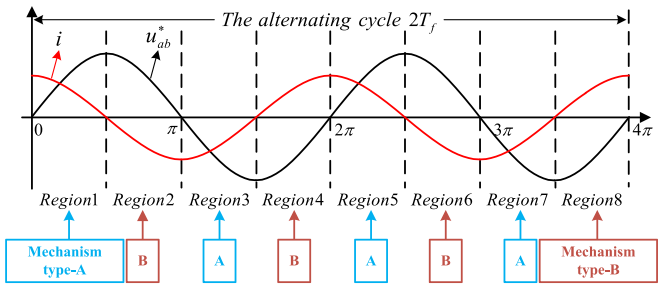

Fig. 6 Proposed alternating operation mechanisms control method for H-bridge converter.

that in region 1, in region 5 the normal PWM operation of the H-bridge converter is achieved by keeping diode D_4 in ON-state, and operating switch S_2 and diode D_1 in switching state. Similarly, the normal PWM operation of the H-bridge converter in region 3 is achieved by keeping diode D_2 in ON-state, and making switch S_4 and diode D_3 operate in switching state, while in region 7, diode D_3 is designed to keep in ON-state, switch S_1 and diode D_2 operate in switching state, as shown in Fig. 7(b) and (d).

Different from mechanism type-A, as shown in Fig. 8, mechanism type-B is designed for regions 2, 4, 6, and 8, which is characterized by keeping one switch in ON-state, and operating its diagonal switch and a diode (from the other power module in the same leg as the diagonal switch) in switching state. From Fig. 8(a) and (c), it can be seen that the normal PWM operation of the H-bridge converter in region 2 can be achieved only by keeping switch S_4 in ON-state, and operate switch S_1 and diode D_2 in switching state, while to make sure to evenly use each power device, in region 6 the PWM operation can be changed to keep switch S_1 in ON-state, and operate switch S_4 and diode D_3 in switching state. Similarly,

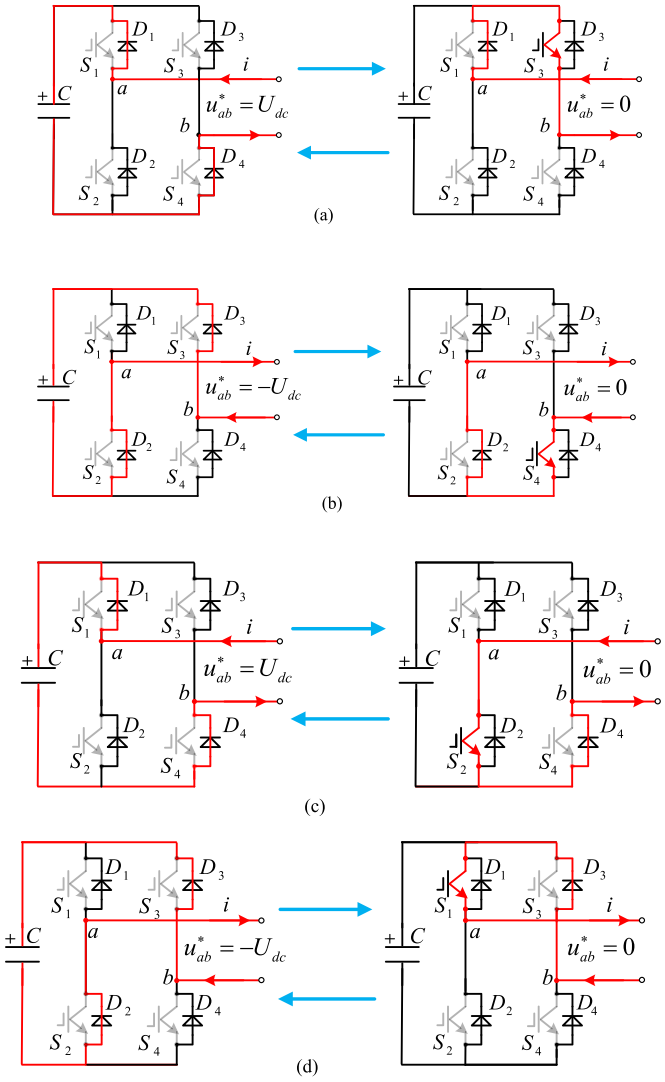

Fig. 7 Novel operation mechanism type-A of the devices in the regions. (a) Region 1. (b) Region 3. (c) Region 5. (d) Region 7. (a) D_1 keeps in on-state, D_4 and S_3 operate in switching state. (b) D_2 keeps in on-state, D_3 and S_4 operate in switching state. (c) D_4 keeps in on-state, D_1 and S_2 operate in switching state. (d) D_3 keeps in on-state, D_2 and S_1 operate in switching state.

the normal PWM operation of the H-bridge converter in region 4 can be achieved by keeping switch S_2 in ON-state, and operating switch S_3 and diode D_4 in switching state, while in region 8, the PWM operation changes to keep switch S_3 in ON-state, and operate switch S_2 and diode D_1 in switching state, as shown in Fig. 8(b) and (d).

Obviously, benefiting from the novel mechanisms type-A and type-B, all active switches and anti-parallel diodes work alternately in these eight regions, each of them is designed to keep in ON-state in one region, operate in switching state in another two regions, and do not work in the left other five regions. In addition to the alternation mode illustrated in Figs. 7 and 8, the proposed PWM method also contains seven other alternation modes, which are all composed of mechanisms type-A and type-B, as shown in Table II. The switching times and mean conduction time of these devices within T_f under the proposed

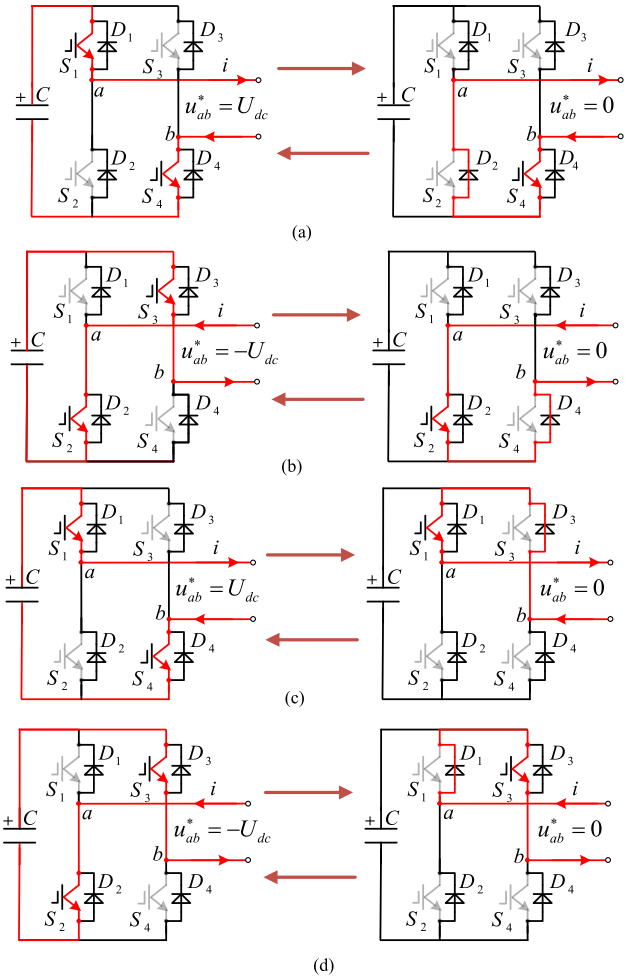

Fig. 8 Novel operation mechanism type-B of the devices in the regions. (a) Region 2. (b) Region 4. (c) Region 6. (d) Region 8. (a) S_4 keeps in on-state, D_2 and S_1 operate in switching state. (b) S_2 keeps in on-state, D_4 and S_3 operate in switching state. (c) S_1 keeps in on-state, D_3 and S_4 operate in switching state. (d) S_3 keeps in on-state, D_1 and S_2 operate in switching state.

method are given by the following equations:

$$N_{\mathrm{sw\_}S_1,S_2,S_3,S_4} = N_{\mathrm{sw\_}D_1,D_2,D_3,D_4} = \frac{T_f}{4T_{\mathrm{sw}}} \tag{6}$$

$$\begin{cases} T_{\mathrm{con\_}S_1,S_2,S_3,S_4} = \frac{(\pi - 2m\cos\theta)}{4\pi} T_f \\ T_{\mathrm{con\_}D_1,D_2,D_3,D_4} = \frac{(\pi + 2m\cos\theta)}{4\pi} T_f. \end{cases} \tag{7}$$

Compared with the conventional PWM methods, the proposed method evenly uses all power devices and effectively reduces their switching times, which will reduce and balance the junction temperature for each device without altering the switching frequency. Besides, since it designs only the necessary devices to work and keeps those unnecessary switches in OFF-state in each region, the proposed method eliminates the requirement of setting a dead-time for the drive signals, which not only improves the power quality and dc-bus voltage utilization of the H-bridge converter, but also avoids the reliability problem caused by simultaneous conduction of the two switches from the same leg.

TABLE II
ENTIRE ALTERNATION MODES OF POWER DEVICES IN THE PROPOSED METHOD

Regions	Alternation mode 1	Alternation mode 2	Alternation mode 3	Alternation mode 4
Region 1	D_1 (keeps in on-state) S_3 and D_4 (operate in switching state) S_4 (keeps in on-state)	D_1 (keeps in on-state) S_3 and D_4 (operate in switching state) S_1 (keeps in on-state)	D_1 (keeps in on-state) S_3 and D_4 (operate in switching state) S_1 (keeps in on-state)	D_1 (keeps in on-state) S_3 and D_4 (operate in switching state) S_4 (keeps in on-state)
Region 2	S_1 and D_2 (operate in switching state) D_2 (keeps in on-state)	S_4 and D_3 (operate in switching state) D_2 (keeps in on-state)	S_4 and D_3 (operate in switching state) D_2 (keeps in on-state)	S_1 and D_2 (operate in switching state) D_2 (keeps in on-state)
Region 3	S_4 and D_3 (operate in switching state) S_3 (keeps in on-state)	S_4 and D_3 (operate in switching state) S_2 (keeps in on-state)	S_4 and D_3 (operate in switching state) S_3 (keeps in on-state)	S_4 and D_3 (operate in switching state) S_2 (keeps in on-state)
Region 4	S_2 and D_1 (operate in switching state) D_4 (keeps in on-state)	S_3 and D_4 (operate in switching state) D_4 (keeps in on-state)	S_2 and D_1 (operate in switching state) D_4 (keeps in on-state)	S_3 and D_4 (operate in switching state) D_4 (keeps in on-state)
Region 5	S_2 and D_1 (operate in switching state) S_1 (keeps in on-state)	S_2 and D_1 (operate in switching state) S_4 (keeps in on-state)	S_2 and D_1 (operate in switching state) S_4 (keeps in on-state)	S_2 and D_1 (operate in switching state) S_1 (keeps in on-state)
Region 6	S_4 and D_3 (operate in switching state) D_3 (keeps in on-state)	S_1 and D_2 (operate in switching state) D_3 (keeps in on-state)	S_1 and D_2 (operate in switching state) D_3 (keeps in on-state)	S_4 and D_3 (operate in switching state) D_3 (keeps in on-state)
Region 7	S_1 and D_2 (operate in switching state) S_2 (keeps in on-state)	S_1 and D_2 (operate in switching state) S_3 (keeps in on-state)	S_1 and D_2 (operate in switching state) S_2 (keeps in on-state)	S_1 and D_2 (operate in switching state) S_3 (keeps in on-state)
Region 8	S_3 and D_4 (operate in switching state)	S_2 and D_1 (operate in switching state)	S_3 and D_4 (operate in switching state)	S_2 and D_1 (operate in switching state)
Regions	Alternation mode 5	Alternation mode 6	Alternation mode 7	Alternation mode 8
Region 1	D_1 (keeps in on-state) S_3 and D_4 (operate in switching state) S_1 (keeps in on-state)	D_1 (keeps in on-state) S_3 and D_4 (operate in switching state) S_4 (keeps in on-state)	D_1 (keeps in on-state) S_3 and D_4 (operate in switching state) S_1 (keeps in on-state)	D_1 (keeps in on-state) S_3 and D_4 (operate in switching state) S_4 (keeps in on-state)
Region 2	S_4 and D_3 (operate in switching state) D_3 (keeps in on-state)	S_1 and D_2 (operate in switching state) D_3 (keeps in on-state)	S_4 and D_3 (operate in switching state) D_3 (keeps in on-state)	S_1 and D_2 (operate in switching state) D_3 (keeps in on-state)
Region 3	S_1 and D_2 (operate in switching state) S_2 (keeps in on-state)	S_1 and D_2 (operate in switching state) S_3 (keeps in on-state)	S_1 and D_2 (operate in switching state) S_3 (keeps in on-state)	S_1 and D_2 (operate in switching state) S_2 (keeps in on-state)
Region 4	S_3 and D_4 (operate in switching state) D_4 (keeps in on-state)	S_2 and D_1 (operate in switching state) D_4 (keeps in on-state)	S_2 and D_1 (operate in switching state) D_4 (keeps in on-state)	S_3 and D_4 (operate in switching state) D_4 (keeps in on-state)
Region 5	S_2 and D_1 (operate in switching state) S_4 (keeps in on-state)	S_2 and D_1 (operate in switching state) S_1 (keeps in on-state)	S_2 and D_1 (operate in switching state) S_4 (keeps in on-state)	S_2 and D_1 (operate in switching state) S_1 (keeps in on-state)
Region 6	S_1 and D_2 (operate in switching state) D_2 (keeps in on-state)	S_4 and D_3 (operate in switching state) D_2 (keeps in on-state)	S_1 and D_2 (operate in switching state) D_2 (keeps in on-state)	S_4 and D_3 (operate in switching state) D_2 (keeps in on-state)
Region 7	S_4 and D_3 (operate in switching state) S_3 (keeps in on-state)	S_4 and D_3 (operate in switching state) S_2 (keeps in on-state)	S_4 and D_3 (operate in switching state) S_2 (keeps in on-state)	S_4 and D_3 (operate in switching state) S_3 (keeps in on-state)
Region 8	S_2 and D_1 (operate in switching state)	S_3 and D_4 (operate in switching state)	S_3 and D_4 (operate in switching state)	S_2 and D_1 (operate in switching state)

C. Implementation Strategy of the Proposed PWM Method

The implementation strategy of the proposed method is shown in Fig. 9, which is designed to provide real-time and accurate drive signals for the power switching devices in each region to make them obtain the novel mechanisms type-A and type-B. The implementation strategy consists of three algorithm components, including DQ current decoupling control algorithm, modulation algorithm, and drive signal selection algorithm.

The DQ current decoupling control algorithm aims at generating the reference voltage signal u_{ab}^{*} required by the subsequent algorithm based on a typical double closed-loop control structure, where the outer loop is used to control the power transmission and the inner loop is used to regulate the current quality.

The modulation algorithm is designed to convert the reference voltage signal u_{ab}^{*} into the modulation signal $|u_{\mathrm{ref}}|$, and then generate the corresponding drive signal by a specific modulation scheme. As shown in Fig. 10, both the modulation and carrier

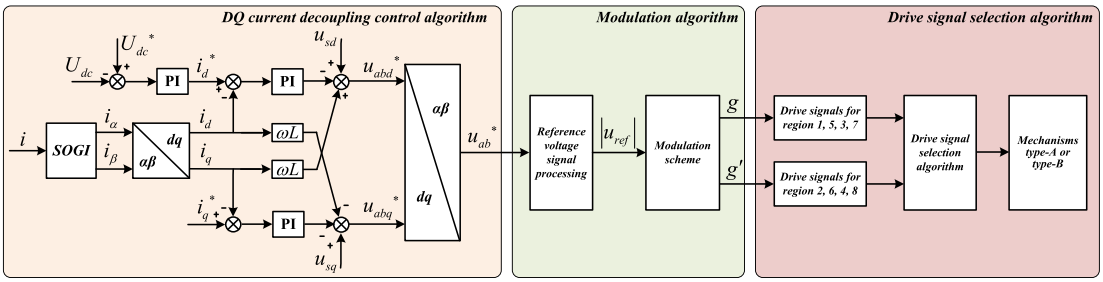

Fig. 9 Control diagram of the corresponding implementation strategy for the proposed method.

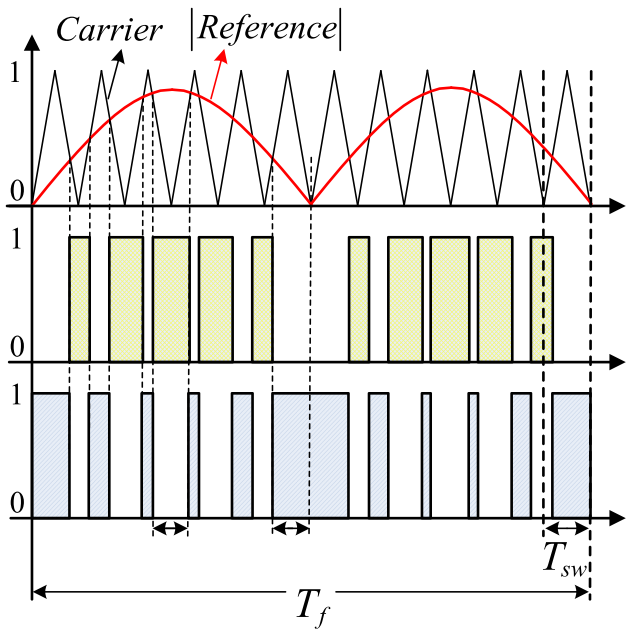

Fig. 10 Modulation algorithm of the implementation strategy.

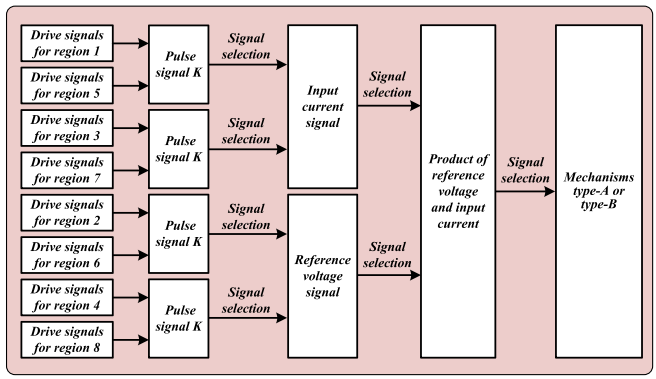

Fig. 11 Drive signal selection algorithm of the implementation strategy.

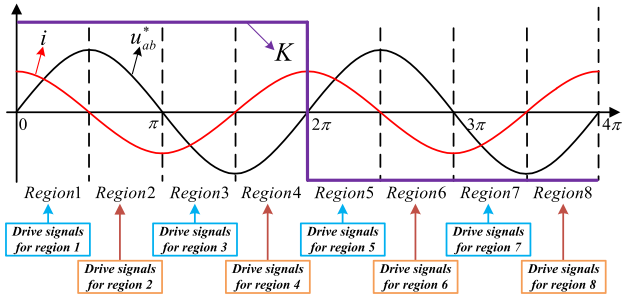

Fig. 12 Principle of three-stage drive signal selector.

signals are set to an absolute value greater than zero, and a pair of complementary drive signals g and g' are generated and utilized to control the specific switches that operate in switching state in regions 2, 4, 6, and 8 and regions 1, 3, 5, and 7. The expressions of $|u_{\text{ref}}|$ are given by the following equation:

$$|u_{\text{ref}}| = \left| \frac{u^*_{ab}}{U_{\text{dc}}} \right| \tag{8}$$

and the conduction time T_g and $T_{g'}$ within one switching cycle T_{sw} are given by the following equation:

$$\begin{cases} T_g = |m \sin(\omega t)| \cdot T_{\text{sw}} \\ T_{g'} = T_{\text{sw}} - |m \sin(\omega t)| \cdot T_{\text{sw}}. \end{cases} \tag{9}$$

As shown in Fig. 11, the drive signal selection algorithm combines the drive signals g and g' with the ON-state and OFF-state drive signals 1 and 0 to form eight sets of novel drive signals corresponding to the eight regions, and subsequently assigns these drive signals to each region precisely by a three-stage signal selector composed of the pulse signal K, the input current, and reference voltage. As depicted in Fig. 12, the pulse signal K is used to distinguish between the first and second fundamental frequency period within an alternating cycle with a pulse frequency that is half of the fundamental frequency. Assume that the H-bridge converter is operating in region 1, at which time $K > 0$, $u^*_{ab} > 0$, $i > 0$, and the product of u^*_{ab} and i are also greater than 0, which means that the first-stage signal selector will pick out the drive signals for regions 1, 2, 3, and 4, the second-stage signal selector further picks out the drive signals for regions 1 and 2, and the third-stage signal selector finally picks out the drive signals for region 1. By means of the drive signal selection algorithm, the power switching devices in each region will obtain the corresponding operating mechanism type-A or type-B in real-time.

Indeed, the proposed PWM method is more complicated than the conventional modulation methods in terms of algorithm design due to the added judgment for different regions of the H-bridge converter, but it is not a burden for the digital controllers (e.g., DSP controllers).

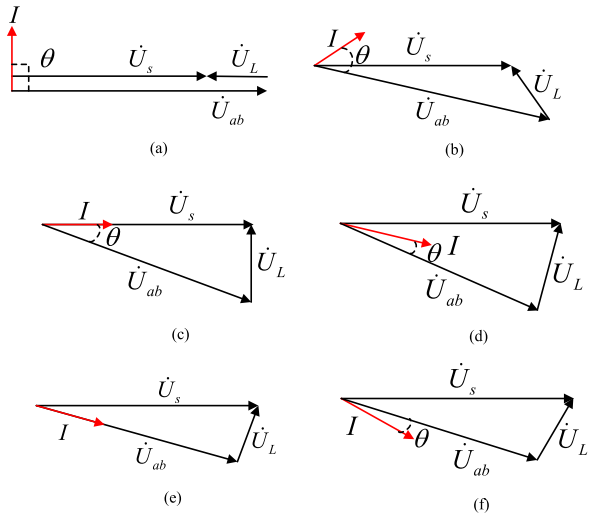

Fig. 13 Phase relations between input current and reference voltage at different power factors of H-bridge converters.

III. Theoretical Losses Analysis

In order to clearly discuss the advantages of the proposed method in terms of losses distribution and its effectiveness at different operating points, a comprehensive losses analysis of power devices under the traditional and proposed methods is presented in follows. The losses that occur in power device can be classified as conduction losses, switching losses, and OFF-state blocking losses, where the last term is usually neglected because the leakage current is of negligible level during the OFF-state.

Conduction losses occur while the power device is in ON-state and conducting current, which are calculated by multiplying the ON-state saturation voltage by the conducting current. The saturation voltage can be approximated as the linear equation of the current that flows through the diodes and switches. The mean conduction losses can be written by the following equation [33], [34]:

$$\begin{cases} P_{\text{con\_Switch}} = \frac{1}{T}\int_{\alpha}^{\beta}\left[(U_{ce0}+R_{ce}\cdot|i|)\cdot i\cdot\lambda_s\right]\cdot d(\omega t) \\ P_{\text{con\_Diode}} = \frac{1}{T}\int_{\alpha}^{\beta}\left[(U_{d0}+R_{d}\cdot|i|)\cdot i\cdot\lambda_d\right]\cdot d(\omega t) \end{cases} \tag{10}$$

where U_{ce0}, U_{d0}, R_{ce}, R_d, and λ_s, λ_d are, respectively, the threshold voltage, equivalent resistance, and duty cycle of switches and diodes, α and β are, respectively, defined as the start phase and end phase of the operation interval of the devices within the cycle.

Switching losses are the power dissipation during turn-ON and turn-OFF switching transitions, which are proportional to the switching frequency. The mean switching losses can be written by the following equation [35], [36]:

$$\begin{cases} P_{\text{sw\_Switch}} = \frac{1}{T}\int_{\alpha}^{\beta}\left(E_{\text{on}}+E_{\text{off}}\right)\cdot f_{\text{sw}}\cdot d(\omega t) \\ P_{\text{sw\_Diode}} = \frac{1}{T}\int_{\alpha}^{\beta}E_{\text{rec}}\cdot f_{\text{sw}}\cdot d(\omega t) \end{cases} \tag{11}$$

where f_{sw} is the switching frequency, $E_{\text{rec}}[J]$, $E_{\text{on}}[J]$, and $E_{\text{off}}[J]$ are respectively reverse recovery energy losses of diodes, turn-ON switching energy losses, and turn-OFF switching energy losses of switches, which are all available in datasheets. In order to unify the calculation, the mean power dissipation of each device is calculated in two fundamental frequency periods.

A. Losses Analysis for Conventional PWM Methods

For bipolar PWM method, the mean conduction and switching losses of each device in two fundamental frequency periods are given by (12) and (13), where the power dissipation of the switches and diodes are equal, respectively.

Due to the identical operation mechanism, the conduction and switching losses of power devices under unipolar-I and-II PWM methods are equivalent to those under bipolar method. Therefore, only the switching and conduction losses under unipolar-III PWM method are discussed in this article, given by (14) and (15). It can be found that the losses distribution under this method is extremely nonuniform and varies with the phase difference θ. Only when $\theta = \pi/2$, the switching losses of switches and diodes are equal, respectively.

$$\begin{cases} P_{\text{sw\_}S_1,S_3} = \frac{\pi-\theta}{2\pi}f_{\text{sw}}\cdot(E_{\text{on}}+E_{\text{off}}) \\ P_{\text{sw\_}S_2,S_4} = \frac{\theta}{2\pi}f_{\text{sw}}\cdot(E_{\text{on}}+E_{\text{off}}) \\ P_{\text{sw\_}D_1,D_3} = \frac{\theta}{2\pi}f_{\text{sw}}\cdot E_{\text{rec}} \\ P_{\text{sw\_}D_2,D_4} = \frac{\pi-\theta}{2\pi}f_{\text{sw}}\cdot E_{\text{rec}} \end{cases} \tag{14}$$

$$\begin{cases} P_{\text{con\_}D_1,D_3} = \frac{U_{d0}I_m}{4\pi}\cdot(4+m\theta\cos\theta-msin\theta) \\ \qquad + \frac{R_dI_m^2}{4\pi}\cdot\left(\pi-m+\frac{4}{3}m\cos\theta-\frac{1}{3}m\cos 2\theta\right) \\ P_{\text{con\_}D_2,D_4} = \frac{U_{d0}I_m}{4\pi}\cdot(m(\pi-\theta)\cos\theta+msin\theta) \\ \qquad + \frac{R_dI_m^2}{4\pi}\cdot\left(m+\frac{4}{3}m\cos\theta+\frac{1}{3}m\cos 2\theta\right) \\ P_{\text{con\_}S_1,S_3} = \frac{U_{ce0}I_m}{4\pi}\cdot(4-m(\pi-\theta)\cos\theta-msin\theta) \\ \qquad + \frac{R_{ce}I_m^2}{4\pi}\cdot\left(\pi-m-\frac{4}{3}m\cos\theta-\frac{1}{3}m\cos 2\theta\right) \\ P_{\text{con\_}S_2,S_4} = \frac{U_{ce0}I_m}{4\pi}\cdot(-m\theta\cos\theta+msin\theta) \\ \qquad + \frac{R_{ce}I_m^2}{4\pi}\cdot\left(m-\frac{4}{3}m\cos\theta+\frac{1}{3}m\cos 2\theta\right). \end{cases} \tag{15}$$

B. Losses Analysis for the Proposed PWM Method

For the proposed PWM method, the mean conduction losses and switching losses are given by (16) and (17), where it can be seen that the losses of the switches and diodes will always be equal, respectively, even if the H-bridge converter works at different operating points (different current magnitude I_m, phase difference θ, fundamental frequency period T_f, and modulation index m).

As shown in Fig. 13(a), when the H-bridge converter operates as a CRPC or IRPC, the input current will either lead reference voltage with the phase difference of $\theta = \pi/2$ (capacitive) or lag it with the same phase difference (inductive), which results in a consistent duration for regions 1/3/5/7 and regions 2/4/6/8.

While making the H-bridge converter operate as a rectifier, three phase relations will appear between the input current and reference voltage which areas follows:

1) The input current leads reference voltage with the phase difference θ (leading power factor, unit power factor and lagging power factor), as shown in Fig. 13(b)–(d).

TABLE III
SIMULATION PARAMETERS OF THE OPERATING POINTS

Simulation parameter	Operating point 1	Operating point 2	Operating point 3	Operating point 4
IGBTs	IKW20N60T	IKW20N60T	IKW20N60T	IKW20N60T
Grid voltage	110Vrms/50Hz	110Vrms/50Hz	110Vrms/50Hz	110Vrms/50Hz
DC-bus voltage	200V	200V	200V	200V
Switching frequency	20kHz	20kHz	20kHz	20kHz
Boost inductor	5mH	5mH	5mH	5mH
DC-bus capacitor	2200μF	2200μF	2200μF	2200μF
Input current	10Arms	10Arms	20Arms	20Arms
Operating mode	CRPC mode (rms current leads grid voltage by $\pi/2$)	Rectifier mode (rms current leads grid voltage by $\pi/6$)	CRPC mode (rms current leads grid voltage by $\pi/2$)	Rectifier mode (rms current lags grid voltage by $\pi/4$)
Ambient temperature	25℃	25℃	25℃	25℃

2) The input current lags reference voltage with the phase difference θ (lagging power factor), as shown in Fig. 13(f).
3) The input current is in phase with reference voltage (lagging power factor), as shown in Fig. 13(e).

Among these phase relations, the phase difference θ always satisfy: $0 \leq \theta < \pi/2$, which makes the duration of regions 1/3/5/7 will be longer than that of regions 2/4/6/8.

Likewise, three different phase relations also exist between the input current and reference voltage when the H-bridge converter operates in inverter mode, where the phase difference θ always satisfies: $\pi/2 < \theta \leq \pi$, which implies that the duration of regions 1/3/5/7 will be shorter than that of regions 2/4/6/8.

Clearly, the power factor changes the phase relation between the input current and reference voltage as well as the duration of each region, but it has no effect on the effectiveness of the proposed method, which is because the conduction and switching losses of the switches and diodes are always equal for all phase differences.

Meanwhile, it follows from (13) to (18), although the losses of power devices under traditional bipolar PWM method are also equal, since the switching losses under the proposed method are only half of that under the bipolar PWM method, the power dissipation and junction temperature of the power switching

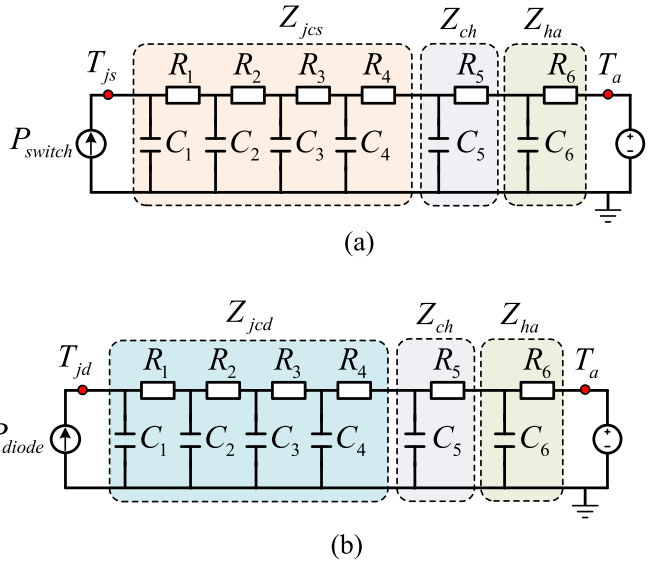

Fig. 14 One-dimensional Cauer-type thermal network of the thermal simulation model. (a) Six-layer RC thermal network of IGBT chip from junction to ambient temperature. (b) Six-layer RC thermal network of anti-parallel diode chip from junction to ambient temperature.

$$\begin{cases} P_{\text{con\_}S_1,S_2,S_3,S_4} = \left(\frac{U_{ce0}I_m}{2\pi} + \frac{R_{ce}I_m^2}{8}\right) - \cos\theta\left(\frac{U_{ce0}I_m m}{8} + \frac{R_{ce}I_m^2 m}{3\pi}\right) \\ P_{\text{con\_}D_1,D_2,D_3,D_4} = \left(\frac{U_{d0}I_m}{2\pi} + \frac{R_d I_m^2}{8}\right) + \cos\theta\left(\frac{U_{d0}I_m m}{8} + \frac{R_d I_m^2 m}{3\pi}\right) \end{cases} \tag{12}$$

$$\begin{cases} P_{\text{sw\_}S_1,S_2,S_3,S_4} = \frac{1}{2} f_{\text{sw}} \cdot (E_{\text{on}} + E_{\text{off}}) \\ P_{\text{sw\_}D_1,D_2,D_3,D_4} = \frac{1}{2} f_{\text{sw}} \cdot E_{\text{rec}}. \end{cases} \tag{13}$$

$$\begin{cases} P_{\text{con\_}S_1,S_2,S_3,S_4} = \left(\frac{U_{ce0}I_m}{2\pi} + \frac{R_{ce}I_m^2}{8}\right) - \cos\theta\left(\frac{U_{ce0}I_m m}{8} + \frac{R_{ce}I_m^2 m}{3\pi}\right) \\ P_{\text{con\_}D_1,D_2,D_3,D_4} = \left(\frac{U_{d0}I_m}{2\pi} + \frac{R_d I_m^2}{8}\right) + \cos\theta\left(\frac{U_{d0}I_m m}{8} + \frac{R_d I_m^2 m}{3\pi}\right) \end{cases} \tag{16}$$

$$\begin{cases} P_{\text{sw\_}S_1,S_2,S_3,S_4} = \frac{1}{4} f_{\text{sw}} \cdot (E_{\text{on}} + E_{\text{off}}) \\ P_{\text{sw\_}D_1,D_2,D_3,D_4} = \frac{1}{4} f_{\text{sw}} \cdot E_{\text{rec}}. \end{cases} \tag{17}$$

TABLE IV
THERMAL RESISTANCE AND CAPACITANCE PARAMETERS FOR SIX-LAYER CAUER THERMAL NETWORK

Layers	Thermal resistance and capacitance for IGBT chip	Thermal resistance and capacitance for diode chip
Layer 1	0.1784 K/W 0.0008207 J/W	0.4251 K/W 0.0003273 J/W
Layer 2	0.2486 K/W 0.00195 J/W	0.4663 K/W 0.00317 J/W
Layer 3	0.3297 K/W 0.03296 J/W	0.5265 K/W 0.03219 J/W
Layer 4	0.1279 K/W 0.4989 J/W	0.08296 K/W 1.065 J/W
Layer 5	1.0 K/W 0.06 J/W	1.0 K/W 0.06 J/W
Layer 6	2.5 K/W 0.12 J/W	2.5 K/W 0.12 J/W

devices under the proposed method will be significantly lower than those under the bipolar method. It should be noted that the conduction and switching losses of power devices are always unequal under the unipolar-III PWM method, which always makes two of the four switching devices (devices 1 and 3, or devices 2 and 4) at a higher temperature. Only when $\theta = \pi/2$, the switching losses under the unipolar-III method are comparable to those under the proposed method.

Therefore, based on the above analysis, compared with the conventional PWM methods, the proposed method can effectively reduce the switching losses by half and distribute the conduction and switching losses uniformly among the power devices, which enables the power switching devices in the H-bridge converter to have a uniform and lower junction temperature and higher reliability. For different operating points (different current magnitudes, power factors, and fundamental frequency periods), the proposed method is always effective.

IV. SIMULATION AND EXPERIMENTAL ANALYSIS

A. *Method Validation Based on Thermal Simulation Model*

A thermal simulation model of the H-bridge converter based on PLECS software is established and implemented to validate the feasibility and effectiveness of the proposed modulation method at different operating points. The selected operating points, whose simulation parameters are listed in Table III, apply the same IGBTs (IKW20N60T), nominal voltage (110 V), and fundamental frequency (50 Hz), 50% and 100% of rms current, as well as three different power factor angles. The rms currents in operating points 1 and 3 are made to lead grid voltage by $\pi/2$ (CRPC mode), while the rms currents in operating point 2 and 4 are made to lead and lag grid voltage by $\pi/6$ and $\pi/4$ (rectifier mode), respectively.

Assuming that the IGBT chip and anti-parallel diode chip have independent heat conduction paths, a series-connected one-dimensional Cauer-type thermal network is introduced to model the thermal behavior of the IGBT (IKW20N60T), thermal grease, and heatsink. As shown in Fig. 14(a) and (b), for IKW20N60T, the transient thermal impedance of both the IGBT chip and diode chip from-junction-to-case Z_{jcs} and Z_{jcd} can be represented by a four-layer Cauer thermal network, where the thermal resistance and capacitance (RC) parameters for each layer are provided by the datasheet. For thermal grease and heatsink, the transient thermal impedance from-case-to-heatsink Z_{ch} and that from-heatsink-to-ambient Z_{ha} are both equivalent to a one-layer Cauer thermal network. Finally, the junction temperature T_{js} and T_{jd} of the IGBT chip and diode chip are connected to the ambient temperature T_a of 25 °C through a six-layer RC thermal network, respectively. The RC parameters for each layer are listed in Table IV.

TABLE V
THD RESULTS OF REFERENCE VOLTAGE AND INPUT CURRENT

Modulation methods	Reference voltage THD	Input current THD
Bipolar PWM method	13.5%	3.9%
Unipolar-III PWM method	8.6%	2.4%
Proposed PWM method	5.7%	1.6%

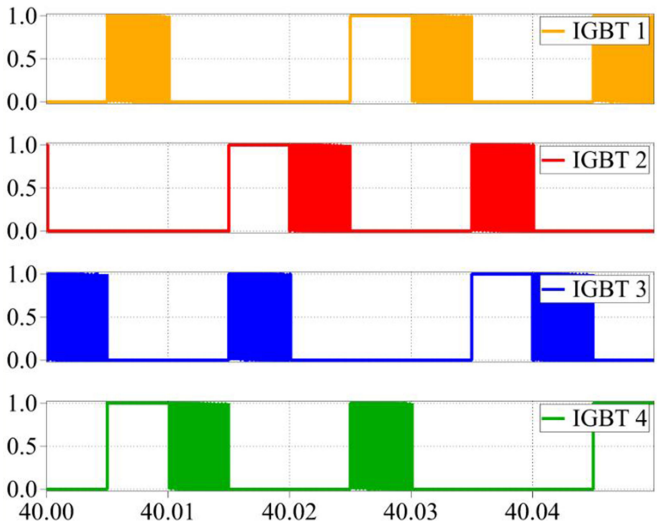

Fig. 15 Drive signals for the IGBTs in the eight regions.

The validation process compares and analyzes the impacts of the conventional PWM methods with a dead-time of 1.5 μsand the proposed method without dead-time on the losses and junction temperatures of IGBTs at these six operating points. The total simulation time is set to 50 s for observing the complete steady-state temperature profiles. The drive signals modulated by the proposed method with a complete alternating cycle (from 40 to 40.04 s) are shown in Fig. 15, where it can be seen that the proposed implementation strategy is capable of obtaining mechanism type-A and type-B accurately for each IGBT, and their alternation mode is consistent with that described in Section II.

Fig. 16 shows the input and output waveforms of the H-bridge converter at the operating point 1 within this alternating

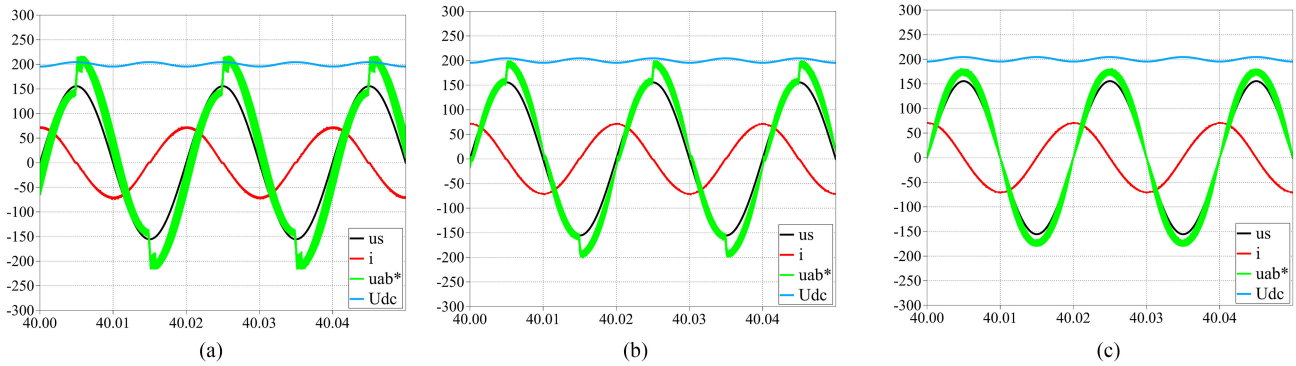

Fig. 16 Input and output waveforms of the H-bridge converter. (a) Under bipolar PWM. (b) Under unipolar-III PWM. (c) Under the proposed PWM.

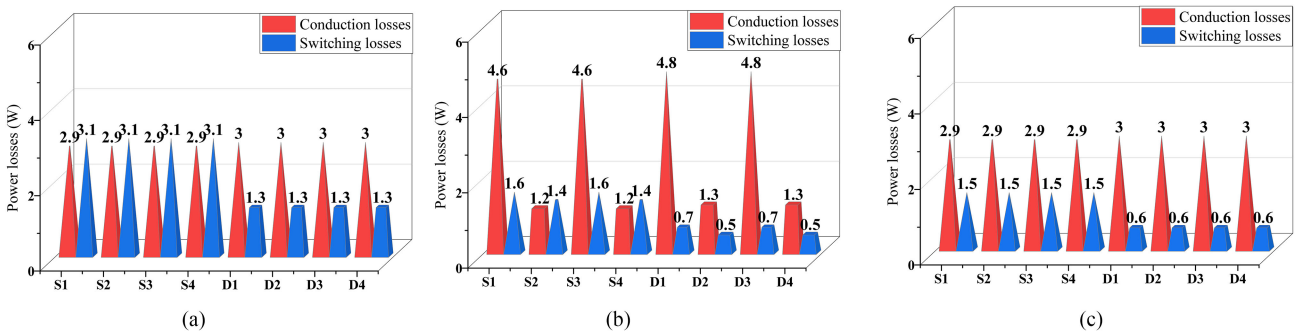

Fig. 17 Conduction and switching losses of IKW20N60Ts at operating point 1. (a) Under bipolar PWM. (b) Under unipolar-III PWM. (c) Under the proposed PWM.

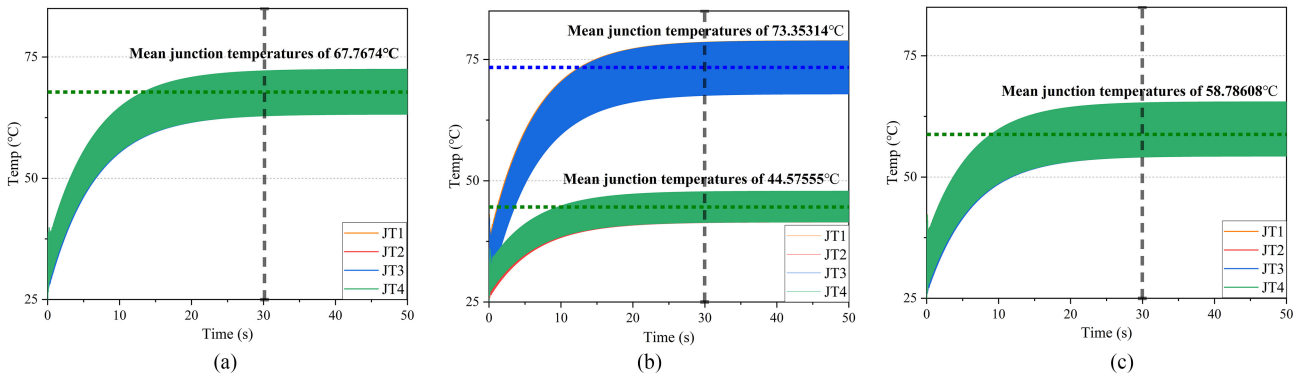

Fig. 18 Junction temperature profiles of IKW20N60Ts at operating point 1. (a) Under bipolar PWM. (b) Under unipolar-III PWM. (c) Under the proposed PWM.

cycle (the current i is amplified by 5 times), where the THD results corresponding to the reference voltage and input current are shown in Table V. Obviously, the conventional PWM methods distort the waveform of reference voltage, while the proposed method improves the output quality of the H-bridge converter.

Fig. 17 shows the conduction and switching losses distribution of IKW20N60T at the operating point 1 under the conventional and proposed modulation methods. Consistent with the results of the theoretical losses analysis, the conduction and switching losses of the switches and diodes under the proposed method are equal, respectively, and the switching losses are only half of those under the bipolar PWM method. For the unipolar-III PWM method, the conduction and switching losses are always nonuniform. By calculation, the power losses of an IGBT under the bipolar PWM method has reached 10.4 W, while it is only 8 W under the proposed method, which is a 23% reduction.

Figs. 18 and 19 show the junction temperature profiles and junction temperature fluctuations of IKW20N60T chip at the operating point 1 under these three modulation methods, respectively, where the junction temperatures enter steady state after 30 s. It can be observed that the mean junction temperatures of the devices under the bipolar PWM method reaches 67.8 °C with a junction temperature fluctuations of 9.2 °C. In contrast, the mean junction temperatures under the proposed method are only 58.8 °C with a junction temperature fluctuations of 8.4 °C.

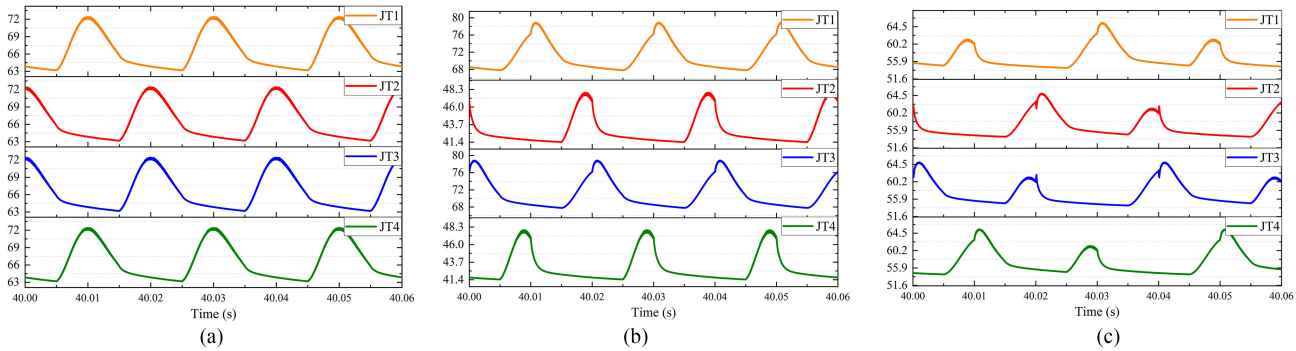

Fig. 19 Junction temperature fluctuations of IKW20N60Ts at operating point 1. (a) Under bipolar PWM. (b) Under unipolar-III PWM. (c) Under the proposed PWM.

TABLE VI
LOSSES AND TEMPERATURES PERFORMANCE OF IKW20N60T AT OPERATING POINTS 1–4

Modulation methods	IGBT losses	Junction temperature range	Mean junction temperature T_m	Temperature fluctuations ΔT_j
Bipolar PWM	10.4W	63.2°C-72.4°C	67.8°C	9.2°C
Unipolar-III PWM	11.6W	67.9°C-79.0°C	73.4°C	11.1°C
	4.5W	41.4°C-47.8°C	44.6°C	6.4°C
Proposed PWM	8.0W	54.6°C-63.0°C	58.8°C	8.4°C
Modulation methods	IGBT losses	Junction temperature range	Mean junction temperature T_m	Temperature fluctuations ΔT_j
Bipolar PWM	10.2W	59.2°C-67.3°C	63.3°C	8.1°C
Unipolar-III PWM	11.4W	64.0°C-71.8°C	67.9°C	7.8°C
	4.7W	40.6°C-42.6°C	41.6°C	2.0°C
Proposed PWM	7.7W	53.4°C-58.7°C	56.0°C	5.3°C
Modulation methods	IGBT losses	Junction temperature range	Mean junction temperature T_m	Temperature fluctuations ΔT_j
Bipolar PWM	26.7W	124.0°C-150.5°C	137.2°C	26.5°C
Unipolar-III PWM	31.2W	140.8°C-175.0°C	157.9°C	34.2°C
	11.4W	67.0°C-84.0°C	75.5°C	17.0°C
Proposed PWM	21.0W	102.6°C-126.5°C	114.5°C	23.9°C
Modulation methods	IGBT losses	Junction temperature range	Mean junction temperature T_m	Temperature fluctuations ΔT_j
Bipolar PWM	26.0W	118°C-136°C	127.0°C	18.0°C
Unipolar-III PWM	32.7W	134°C-156°C	145.0°C	22.0°C
	9.2W	60°C-69.6°C	64.8°C	9.6°C
Proposed PWM	20.5W	98.8°C-114°C	106.4°C	15.2°C

Meanwhile, the unipolar-III PWM method suffers the devices from the issue of uneven junction temperature distribution, which makes this method unsuitable for utility. Obviously, the proposed method balances the junction temperature distribution for all IGBTs compared with the unipolar-III PWM method, and reduces the mean junction temperature by 9 °C compared with the bipolar PWM method without increasing the junction temperature fluctuations. Furthermore, although the proposed method currently lacks the ability to actively control junction temperature fluctuations, the amplitude of junction temperature fluctuation decreases as the mean junction temperature reduces, thus smoothing the junction temperature fluctuations passively.

Table VI summarizes the losses and junction temperature information of IKW20N60T at operating points 1–4 based on different modulation methods, where the power losses are reduced by 23%, 24.5%, 21.3%, and 21.1%, respectively, and also the mean junction temperatures are reduced by 9, 7.3, 22.7,

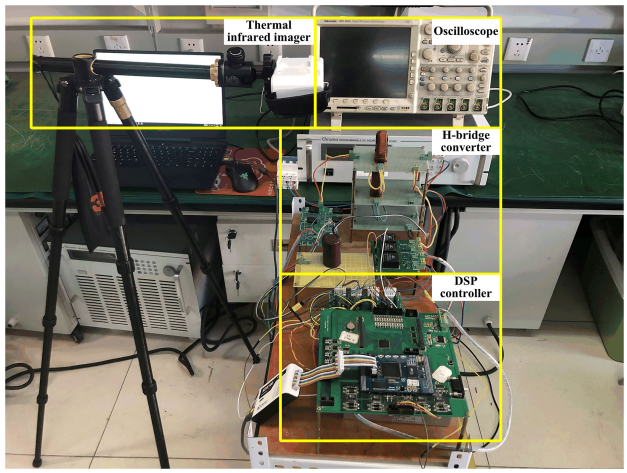

Fig. 20 Laboratory prototype consisting of thermal infrared imager, H-bridge converter, and DSP controller.

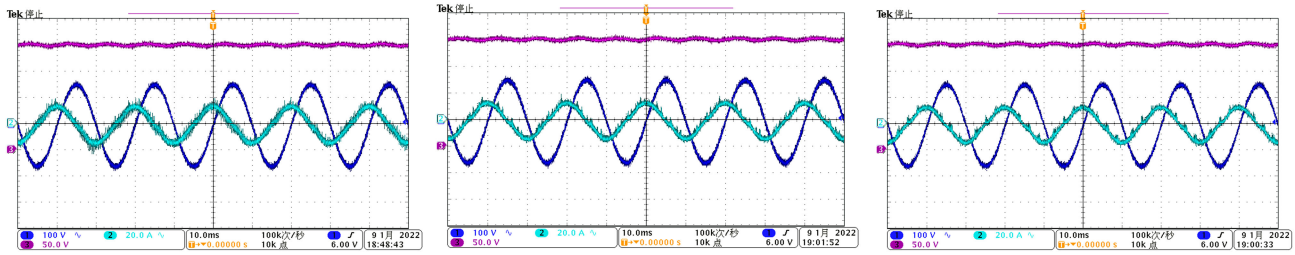

(a) (b) (c)

Fig. 21 AC-side and dc-side waveforms of the H-bridge converter at operating point 1. (a) Under bipolar PWM. (b) Under unipolar-III PWM. (c) Under the proposed PWM.

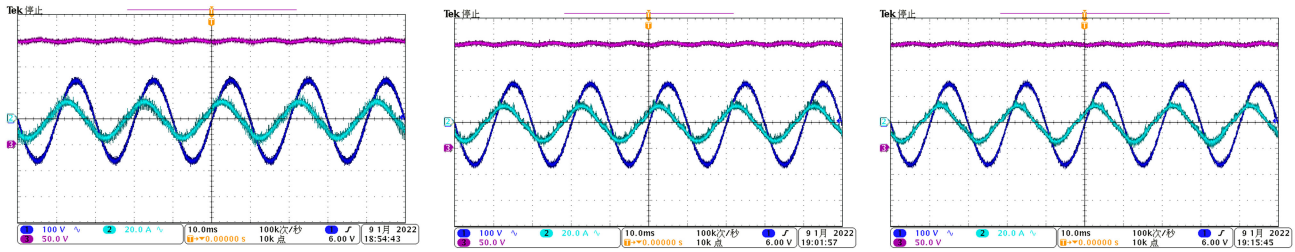

(a) (b) (c)

Fig. 22 AC-side and dc-side waveforms of the H-bridge converter at operating point 2. (a) Under bipolar PWM. (b) Under unipolar-III PWM. (c) Under the proposed PWM.

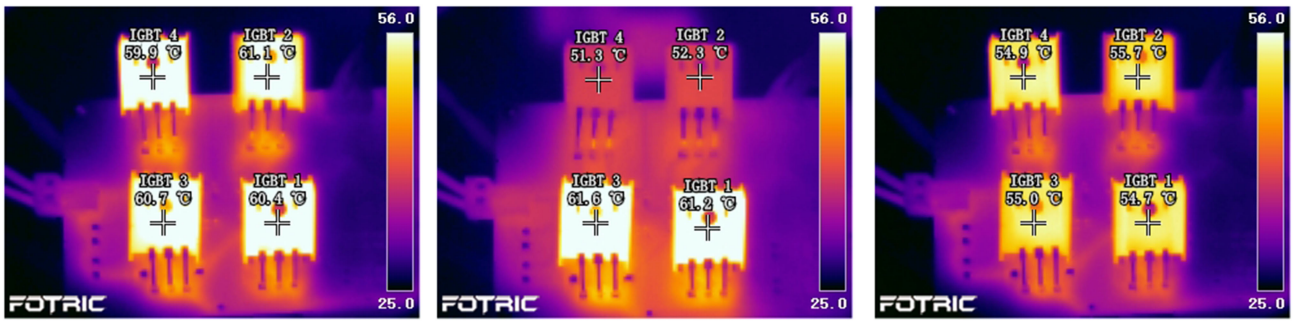

(a) (b) (c)

Fig. 23 Thermal images of the steady-state case temperature of IKW20N60Ts at operating point 1. (a) Under bipolar PWM. (b) Under unipolar-III PWM. (c) Under the proposed PWM.

and 20.6 °C, respectively. These results demonstrate that the proposed method has a general and significant effect on reducing and balancing the losses and junction temperature of power switching devices.

B. Method Validation Based on Laboratory Prototype

To further verify the effectiveness of the proposed method, a laboratory prototype composed of thermal infrared imager, H-bridge converter, and DSP controller is built, as shown in Fig. 20. The IGBT devices and their corresponding operating points adopted in the laboratory prototype are same as those in the simulation model, where the IGBTs are assembled with identical heatsinks via thermal grease and heat dissipated by air-cooling. Since the junction temperatures of the IGBTs are unavailable to be measured, a thermal infrared imager is utilized to measure and record their case temperature performances in real-time.

Figs. 21 and 22 show the ac-side and dc-side waveforms of the H-bridge converter at the operating points 1 and 2 based on the conventional and proposed modulation methods, respectively. As can be seen, the proposed method not only inherently avoids the issue of bridge shoot-through, but also effectively guarantees the output quality of the H-bridge converter, which is not achieved by the conventional PWM methods.

Figs. 23 and 24 show the steady-state case temperatures of IKW20N60Ts corresponding to the operating points 1 and 2, respectively. In agreement with the theoretical losses analysis results and simulation results, all the IGBTs can obtain a lower (compared to bipolar method) and balanced (compared to

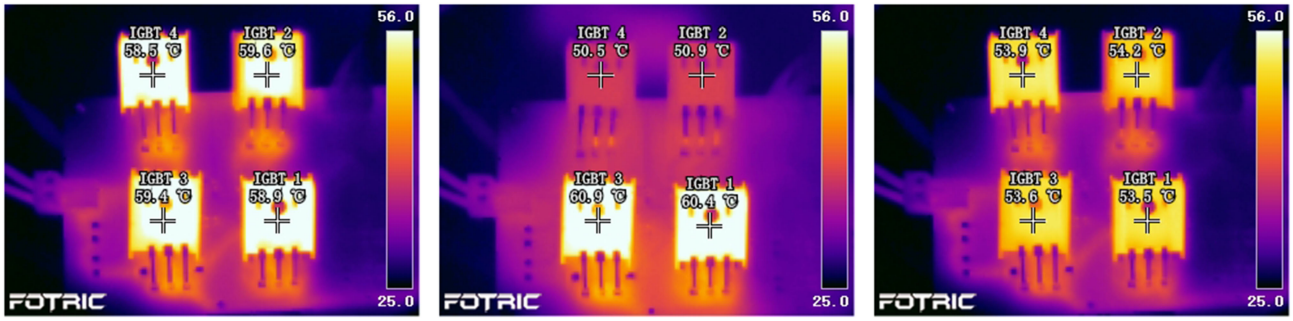

(a) (b) (c)

Fig. 24 Thermal images of the steady-state case temperature of IKW20N60Ts at operating point 2. (a) Under bipolar PWM. (b) Under unipolar-III PWM. (c) Under the proposed PWM.

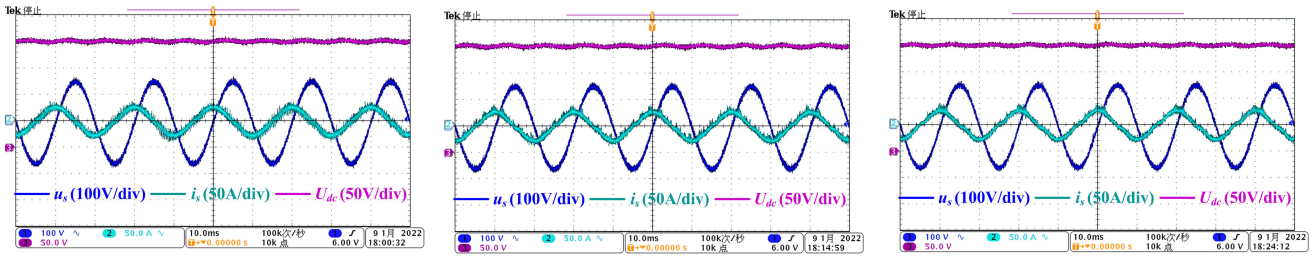

(a) (b) (c)

Fig. 25 AC-side and dc-side waveforms of the H-bridge converter at operating point 3. (a) Under bipolar PWM. (b) Under unipolar-III PWM. (c) Under the proposed PWM.

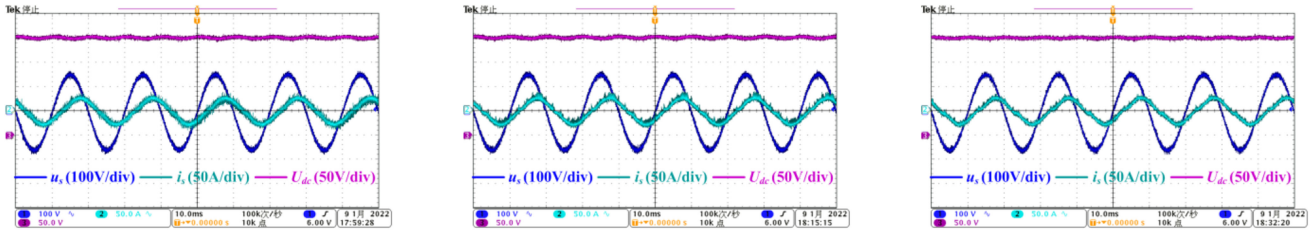

(a) (b) (c)

Fig. 26 AC-side and dc-side waveforms of the H-bridge converter at operating point 4. (a) Under bipolar PWM. (b) Under unipolar-III PWM. (c) Under the proposed PWM.

unipolar method) temperature performance under the proposed modulation method.

For IKW20N60Ts at operating point 1, the proposed method results in a mean case temperature of 55.1 °C, which is about 5.4 °C lower than the mean case temperature of 60.5 °C under the bipolar method.

For IKW20N60Ts at operating point 2, the proposed method results in a mean case temperature of 53.8 °C, which is about 5.1 °C lower than the mean case temperature of 58.9 °C under the bipolar method.

Likewise, Figs. 25 and 26 show the ac-side and dc-side waveforms of the H-bridge converter at the operating points 3 and 4, as well as Figs. 27 and 28 show the corresponding case temperatures of IKW20N60Ts.

For IKW20N60Ts at operating point 3, the proposed method results in a mean case temperature of 70.9 °C, which is about 6.8 °C lower than the mean case temperature of 77.7 °C under the bipolar method.

For IKW20N60Ts at operating point 4, the proposed method results in a mean case temperature of 69.2 °C, which is about 7.3 °C lower than the mean case temperature of 76.5 °C under the bipolar method.

In addition, the case temperatures of IGBT 1 and 3 are significantly higher than those of IGBT 2 and 4 under the unipolar-III method, which makes this method unsuitable for application. Obviously, compared with the conventional modulation methods, the proposed modulation method effectively reduces and evenly distributes the case temperatures of the IGBTs, which not only balances and minimizes the losses and temperature rise of the IGBTs, but also further increases the power density of the H-bridge converter by downsizing the heatsink.

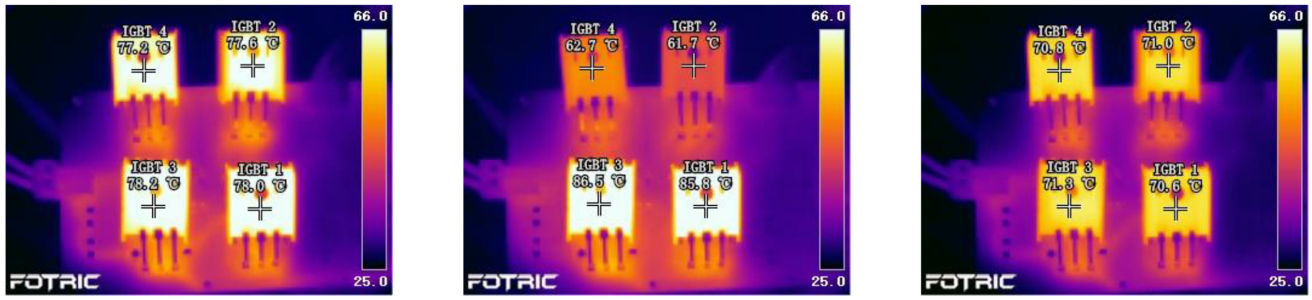

(a) (b) (c)

Fig. 27 Thermal images of the steady-state case temperature of IKW20N60Ts at operating point 3. (a) Under bipolar PWM. (b) Under unipolar-III PWM. (c) Under the proposed PWM.

(a) (b) (c)

Fig. 28 Thermal images of the steady-state case temperature of IKW20N60Ts at operating point 4. (a) Under bipolar PWM. (b) Under unipolar-III PWM. (c) Under the proposed PWM.

V. Conclusion

To address the temperature rise and thermal control issues of power devices in H-bridge converters under conventional PWM methods, this article proposes a novel PWM method for the H-bridge converter with temperature rise balancing and minimization based on periodically alternating employment of power devices. In the proposed method, two novel operation mechanisms of power devices are alternately applied into the eight regions in two fundamental frequency periods. Among them, mechanism type-A is applied to four of the eight regions, where the reference voltage and input current have identical polarities, while mechanism type-B is applied to another four regions, where the reference voltage and input current have opposite polarities. During the entire operation period, all the power devices in H-bridge converters are made to work alternately in the eight regions, each of them is designed to keep in ON-state in one region, operate in switching state in another two regions, and do not work in the left other five regions. By this way, the power dissipation and temperature rise of all the devices are balanced and minimized, and H-bridge converters no longer suffer from the dead-time effect on the output quality and dc-bus voltage utilization. In this article, not only the novel mechanisms in the proposed method is described in detail, but also the losses and temperature performance of power switching devices under the conventional and proposed PWM methods are analyzed and compared. Simulation and experimental results have verified the feasibility and effectiveness of the proposed method at different operating points.

References

[1] G. P. Adam, I. A. Abdelsalam, K. H. Ahmed, and B. W. Williams, "Hybrid multilevel converter with cascaded H-bridge cells for HVDC applications: Operating principle and scalability," *IEEE Trans. Power Electron.*, vol. 30, no. 1, pp. 65–77, Jan. 2015.

[2] A. Moeini and S. Wang, "A DC link sensor-less voltage balancing technique for cascaded H-bridge multilevel converters with asymmetric selective harmonic current mitigation-PWM," *IEEE Trans. Power Electron.*, vol. 33, no. 9, pp. 7571–7581, Sep. 2018.

[3] X. Ge and F. Gao, "Flexible third harmonic voltage control of low capacitance cascaded H-bridge STATCOM," *IEEE Trans. Power Electron.*, vol. 33, no. 3, pp. 1884–1889, Mar. 2018.

[4] G. Farivar, C. D. Townsend, B. Hredzak, J. Pou, and V. G. Agelidis, "Low-Capacitance cascaded H-bridge multilevel statcom," *IEEE Trans. Power Electron.*, vol. 32, no. 3, pp. 1744–1754, Mar. 2017.

[5] W. Huo, B. Sun, and J. Gao, "Research on high power factor control strategy of single-phase electroless capacitor variable frequency speed regulation system," in *Proc. Asia-Pac. Conf. Image Process., Electron. Comput.*, 2020, pp. 242–245.

[6] X. Wang, J. Liu, S. Ouyang, T. Xu, F. Meng, and S. Song, "Control and experiment of an H-bridge-based three-phase three-stage modular power electronic transformer," *IEEE Trans. Power Electron.*, vol. 31, no. 3, pp. 2002–2011, Mar. 2016.

[7] C. Wang, Y. Zhuang, J. Jiao, H. Zhang, C. Wang, and H. Cheng, "Topologies and control strategies of cascaded bridgeless multilevel rectifiers," *IEEE J. Emerg. Sel. Topics Power Electron.*, vol. 5, no. 1, pp. 432–444, Mar. 2017.

[8] S. Du, J. Liu, J. Lin, and Y. He, "A novel DC voltage control method for STATCOM based on hybrid multilevel H-bridge converter," *IEEE Trans. Power Electron.*, vol. 28, no. 1, pp. 101–111, Jan. 2013.

[9] D. Lu, J. Zhu, J. Wang, J. Yao, S. Wang, and H. Hu, "A simple zero-sequence-voltage-based cluster voltage balancing control and the negative sequence current compensation region identification for star-connected cascaded H-bridge STATCOM," *IEEE Trans. Power Electron.*, vol. 33, no. 10, pp. 8376–8387, Oct. 2018.
[10] E. Behrouzian, M. Bongiorno, and R. Teodorescu, "Impact of switching harmonics on capacitor cells balancing in phase-shifted PWM-Based cascaded H-bridge STATCOM," *IEEE Trans. Power Electron.*, vol. 32, no. 1, pp. 815–824, Jan. 2017.
[11] R. Zeng, L. Xu, L. Yao, and B. W. Williams, "Design and operation of a hybrid modular multilevel converter," *IEEE Trans. Power Electron.*, vol. 30, no. 3, pp. 1137–1146, Mar. 2015.
[12] P. M. Meshram and V. B. Borghate, "A simplified nearest level control (NLC) voltage balancing method for modular multilevel converter (MMC)," *IEEE Trans. Power Electron.*, vol. 30, no. 1, pp. 450–462, Jan. 2015.
[13] M. Chai, N. B. Y. Gorla, and S. K. Panda, "Fault detection and localization for cascaded H-bridge multilevel converter with model predictive control," *IEEE Trans. Power Electron.*, vol. 35, no. 10, pp. 10109–10120, Oct. 2020.
[14] M. Aleenejad, H. Mahmoudi, and R. Ahmadi, "Unbalanced space vector modulation with fundamental phase shift compensation for faulty multilevel converters," *IEEE Trans. Power Electron.*, vol. 31, no. 10, pp. 7224–7233, Oct. 2016.
[15] S. Peyghami, Z. Wang, and F. Blaabjerg, "A guideline for reliability prediction in power electronic converters," *IEEE Trans. Power Electron.*, vol. 35, no. 10, pp. 10958–10968, Oct. 2020.
[16] D. Xiang, L. Ran, P. Tavner, S. Yang, A. Bryant, and P. Mawby, "Condition monitoring power module solder fatigue using inverter harmonic identification," *IEEE Trans. Power Electron.*, vol. 27, no. 1, pp. 235–247, Jan. 2012.
[17] B. Wang, J. Cai, X. Du, and L. Zhou, "Review of power semiconductor device reliability for power converters," *CPSS Trans. Power Electron. Appl.*, vol. 2, no. 2, pp. 101–117, 2017.
[18] D. Xiong *et al.*, " Multi-time scale lifetime evaluation of IGBT modules in the wind power converter," *Proc. CSEE*, vol. 35, no. 23, pp. 6152–6161, 2015.
[19] M. Andresen, G. Buticchi, J. Falck, M. Liserre, and O. Muehlfeld, "Active thermal management for a single-phase H-bridge inverter employing switching frequency control," in *Proc. Int. Exhib. Conf. Power Electron., Intell. Motion, Renewable Energy Energy Manage.*, 2015, pp. 1–8.
[20] J. Wu *et al.*, "Smooth control of insulated gate bipolar transistors junction temperature in a small-scale wind power converter," *IET Power Electron.*, vol. 9, no. 3, pp. 393–400, 2016.
[21] L. Wu and A. Castellazzi, "Temperature adaptive driving of power semiconductor devices," in *Proc. IEEE Int. Symp. Ind. Electron.*, 2010, pp. 1110–1114.
[22] P. K. Prasobhu, G. Buticchi, S. Brueske, and M. Liserre, "Gate driver for the active thermal control of a DC/DC gan-based converter," in *Proc. IEEE Energy Convers. Congr. Expo.*, 2016, pp. 1–8.
[23] K. Ma, M. Liserre, and F. Blaabjerg, "Reactive power influence on the thermal cycling of multi-MW wind power inverter," *IEEE Trans. Ind. Appl.*, vol. 49, no. 2, pp. 922–930, Mar./Apr. 2013.
[24] J. Lemmens, P. Vanassche, and J. Driesen, "Optimal control of traction motor drives under electrothermal constraints," *IEEE J. Emerg. Sel. Topics Power Electron.*, vol. 2, no. 2, pp. 249–263, Jun. 2014.
[25] J. Lemmens, J. Driesen, and P. Vanassche, "Thermal management in traction applications as a constraint optimal control problem," in *Proc. IEEE Veh. Power Propulsion Conf.*, 2012, pp. 36–41.
[26] L. Wei, J. McGuire, and R. A. Lukaszewski, "Analysis of PWM frequency control to improve the lifetime of PWM inverter," *IEEE Trans. Ind. Appl.*, vol. 47, no. 2, pp. 922–929, Mar./Apr. 2011.
[27] J. Lemmens, J. Driesen, and P. Vanassche, "Dynamic DC-link voltage adaptation for thermal management of traction drives," in *Proc. IEEE Energy Convers. Congr. Expo.*, 2013, pp. 180–187.
[28] L. Wei, J. M. C. Guire, and J. Hu, "Novel discontinuous PWM control method to improve IGBT reliability at low speed," in *Proc. IEEE Energy Convers. Congr. Expo.*, 2014, pp. 3819–3825.
[29] A. Isidori, F. M. Rossi, F. Blaabjerg, and K. Ma, "Thermal loading and reliability of 10-MW multilevel wind power converter at different wind roughness classes," *IEEE Trans. Ind. Appl.*, vol. 50, no. 1, pp. 484–494, Jan./Feb. 2014.
[30] L. Dalessandro, S. D. Round, U. Drofenik, and J. W. Kolar, "Discontinuous space-vector modulation for three-level PWM rectifiers," *IEEE Trans. Power Electron.*, vol. 23, no. 2, pp. 530–542, Mar. 2008.
[31] Y. Ko, M. Andresen, G. Buticchi, and M. Liserre, "Thermally compensated discontinuous modulation strategy for cascaded H-bridge converters," *IEEE Trans. Power Electron.*, vol. 33, no. 3, pp. 2704–2713, Mar. 2018.
[32] Y. Ko, M. Andresen, G. Buticchi, and M. Liserre, "Discontinuous-modulation-based active thermal control of power electronic modules in wind farms," *IEEE Trans. Power Electron.*, vol. 34, no. 1, pp. 301–310, Jan. 2019.
[33] L. K. Mestha and P. D. Evans, "Analysis of on-state losses in PWM inverters," *IEE Proc. B, Elect. Power Appl.*, vol. 136, no. 4, pp. 189–195, Jul. 1989.
[34] T.-J. Kim, D.-W. Kang, Y.-H. Lee, and D.-S. Hyun, "The analysis of conduction and switching losses in multi-level inverter system," in *Proc. IEEE 32nd Annu. Power Electron. Spec. Conf.*, 2001, vol. 3, pp. 1363–1368.
[35] M. H. Bierhoff and F. W. Fuchs, "Semiconductor losses in voltage source and current source IGBT converters based on analytical derivation," in *Proc. IEEE 35th Annu. Power Electron. Spec. Conf.*, 2004, vol. 4, pp. 2836–2842.
[36] H. V. Nguyen and D. Lee, "Comparison of power losses in single-phase to three-phase AC/DC/AC PWM converters," in *Proc. 9th Int. Conf. Power Electron. ECCE Asia*, 2015, pp. 940–945.

Cong Wang was born in Beijing, China, in 1955. He received the B.S. degree in electrical engineering from the Taiyuan University of Technology, Taiyuan, China, in 1982, and the M.S. and Ph.D. degrees in electrical engineering from the China University of Mining and Technology, Beijing, in 1984 and 2005, respectively.

From 1990 to 1991, he was a Visiting Scholar with the University of Bristol, Bristol, U.K. From 2002 to 2003, he was a Senior Visiting Scholar and a Visiting Professor with the University of Tennessee, Knoxville, TN, USA. He is currently a Professor of Power Electronics with the School of Mechanical Electronic and Information Engineering, China University of Mining and Technology. His current research interests include high power multilevel converters, high-frequency soft-switching converters, and power electronics in smart grid.

Changgeng Tian was born in DaTong, China, in 1989. He received the B.S. degree in electrical engineering from the North China Institute of Science and Technology, Beijing, China, in 2012. He is currently working toward the doctoral degree in power electronics in the School of Mechanical Electronic and Information Engineering, China University of Mining and Technology, Beijing.

His current research interests include high power multilevel converters, power quality mitigation of unidirectional power flow converters, and reliability improvement of power electronic converters.

Hong Cheng was born in Jinhua, China, in 1966. She received the B.S. degree in electrical engineering from Beihang University, Beijing, China, in 1988, and the Ph.D. degree in electrical engineering from the China University of Mining and Technology, Beijing, in 1993.

She is currently a Professor of Power Electronics with the School of Mechanical Electronic and Information Engineering, China University of Mining and Technology. Her current research interests include high power multilevel converters, modeling and control of switching converters, and fault diagnosis of power electronics equipment.

Jiaqing Deng was born in Jiaozuo, China, in 1990. She received the B.S. degree in electrical engineering and automation from Henan Polytechnic University, Jiaozuo, in 2014. She is currently working toward the Ph.D. degree in the School of Mechanical Electronic and Information Engineering, China University of Mining and Technology, Beijing, China.

Her current research interests include high power multilevel converters, high voltage converters, and power electronics in smart grid.